Analytical and Bioanalytical Chemistry
https://doi.org/10.1007/s00216-018-1048-0

PAPER IN FOREFRONT

Carbodiimide-mediated immobilization of acidic biomolecules on reversed-charge zwitterionic sensor chip surfaces

Fabian Risse[1] · Erk T. Gedig[1] · Jochen S. Gutmann[2,3]

Received: 19 December 2017 / Revised: 15 February 2018 / Accepted: 27 March 2018

Abstract

The carbodiimide-mediated amine coupling of protein ligands to sensor chips coated with anionic polycarboxylate hydrogels, such as carboxymethyl dextran, is the predominant covalent immobilization procedure utilized in optical biosensors, namely surface plasmon resonance (SPR) biosensors. Usually, electrostatic interactions at a slightly acidic pH and low ionic strength are employed to efficiently accumulate neutral and basic ligands on the chip surface, which are then covalently coupled by surface-bound active *N*-hydroxysuccinimide (NHS) esters. Unfortunately, this approach is not suitable for acidic proteins or other ligands with low isoelectric points (IEPs), such as nucleic acids, because the charge density of the polycarboxylates is greatly reduced at acidic pH or because electrostatic attraction cannot be achieved. To overcome these drawbacks, we have established a charge-reversal approach that allows the preconcentration of acidic proteins above their IEPs. A precisely controlled amount of tertiary amines is applied to reverse the previous anionic surface charge while maintaining carbodiimide compatibility with future protein immobilization. The mechanism of this reversed-charge immobilization approach was demonstrated employing protein A as a model protein and using attenuated total reflectance Fourier transform infrared spectroscopy, dynamic contact angle measurements, colorimetric quantification, and SPR analysis to characterize surface derivatization. Furthermore, even though it had previously proven impossible to preconcentrate DNA electrostatically and to covalently couple it to polyanionic chip surfaces, we demonstrated that our approach allowed DNA to be preconcentrated and immobilized in good yields.

Keywords Optical biosensor · SPR · Carbodiimide chemistry · Reversed-charge preconcentration · DNA coupling

Introduction

Ion exchange chromatography (IEC) is a popular procedure for the separation and purification of proteins and other charged biomolecules [1], with an underlying principle that has been successfully applied to optical biosensors that use electrostatic preconcentration. Under low ionic strength conditions and pH values at which the stationary phase and the protein have opposite charges, the protein can adsorb on the ion exchanger, releasing counterions. Depending on the charge characteristics, a change in pH and/or an increase in ionic strength can lead to protein desorption [2, 3].

Optical biosensors such as surface plasmon resonance (SPR) sensors [4–7] that are coated with a polyanionic 3D hydrogel such as carboxymethyl dextran (CMD) or polyacrylic acid (PAA) can accumulate proteins from solution under low ionic strength conditions, under which the hydrogel and protein are oppositely charged [8–10]. This process typically leads to multiple layers of adsorbed proteins from a low-concentration ligand solution. Although preconcentration in biosensors is rather similar to electrostatic adsorption in IEC in terms of the principle involved, they have different purposes because proteins need to be covalently immobilized to the sensor surface to allow subsequent biomolecular

Electronic supplementary material The online version of this article (https://doi.org/10.1007/s00216-018-1048-0) contains supplementary material, which is available to authorized users.

✉ Erk T. Gedig
gedig@xantec.com

✉ Jochen S. Gutmann
jochen.gutmann@uni–due.de

[1] XanTec bioanalytics GmbH, Merowingerplatz 1a, 40225 Düsseldorf, Germany

[2] Department of Chemistry and Center for Nanointegration Duisburg-Essen (CENIDE), University Duisburg-Essen, Universitätsstr. 5, 45117 Essen, Germany

[3] Deutsches Textilforschungszentrum Nord-West e.V., Adlerstr. 1, 47798 Krefeld, Germany

Published online: 30 April 2018

interaction analysis in biosensor applications. In this context, amine coupling via reactive esters has become the most frequently used immobilization method, mainly due to its flexibility, ease of use, and high yields [11]. In a first step, inert carboxyl groups in the sensor matrix are transformed into reactive 1-ethyl-3-(3-dimethylaminopropyl)carbodiimide (EDC)-mediated *N*-hydroxysuccinimide (NHS) esters [9, 12]. In a second step, these esters react with nucleophilic groups in the protein (mainly the N-terminus of the protein and NH_2 groups in lysine residues [12]), resulting in stable covalent amide bonds. The latter step requires care, as the reaction can only take place when the protein is in close proximity to the surface-bound NHS esters. This is usually achieved through the electrostatic preconcentration of the protein in the sensor matrix, as previously described [8, 9].

This combination of electrostatic preconcentration and amine coupling via EDC/NHS chemistry is well established, and has become the method of choice to obtain high coupling yields on biosensor surfaces and avoid wasting the often costly protein. However, the limitations of this approach become apparent when the isoelectric point (IEP) of the ligand is low [7, 9]. As the pK_a values of typical polyelectrolytes (such as CMD and PAA) are estimated to be between 3.3 and 4.5, electrostatic preconcentration becomes challenging for proteins with IEPs below 4.5, and is unusable for proteins with IEPs below 4. At lower pH values, extensive optimization experiments may be necessary to realize acceptable adsorption levels due to the reduced surface charge resulting from carboxyl group protonation, while increasing the pH value reduces the positive charge of the protein. For another class of anionic biomolecules, namely DNA and RNA (which includes the emerging subclass of DNA aptamers), electrostatic preconcentration is not applicable, meaning that alternative, less efficient immobilization strategies must be used [13–15]. Furthermore, acidic reaction conditions should be avoided, as the reactivity of NHS esters towards amines is greatly reduced at pH values below 5. Due to the higher percentage of deprotonated amine residues, pH values above 7 are generally preferred, and result in significantly higher coupling yields [9, 12].

The drawbacks described above have limited the use of EDC/NHS coupling in biosensors for almost three decades. Herein, we present a convenient approach for obtaining high covalent-coupling yields of even highly acidic proteins and amino-modified DNA oligos using the well-established technique of EDC/NHS-mediated amine coupling in combination with electrostatic preconcentration on reversed-charge polyanionic hydrogels. This concept is based on the initial condensation of *N*,*N*-dimethylethylenediamine (DMEN), an asymmetric diamine comprising a reactive primary amine and an unreactive cationic tertiary amine, with the carboxyl groups of a PAA hydrogel coating. Given that amidation leads to a loss in charge for both interactants (carboxyl and amine), DMEN introduces a positive charge due to its additional tertiary amine. Moreover, assuming that more than 50% of the carboxyl groups can be transformed into cationic amino derivatives, the surface presumably undergoes charge reversal at physiological pH values. A schematic of this procedure and its proposed combination with amine coupling is shown in Scheme 1.

The scope of this work illustrates that charge reversal in the sensor matrix can be utilized to preconcentrate acidic ligands above their IEP while allowing conventional amine coupling. In this context, we initially evaluated suitable derivatization conditions to generate a reversed-charge sensor surface. Commercially available PAA sensor chips from XanTec (PAA sensor chips consist of a 3D brush-like hydrogel structure comprising high-molecular-weight linear polyacrylic acid attached to a SPR-compatible gold chip) were used as a basic coating platform throughout all experiments, as other weak polyanionic hydrogels might not be suitable due to an insufficient degree of COOH conversion into active esters [9, 16]. Surface characterization based on attenuated total reflectance Fourier transform infrared spectroscopy (ATR-FTIR), colorimetric quantification, zeta potential, and dynamic contact angle measurements was used to classify the derivatization results. Subsequently, the concept of charge reversal was applied to the immobilization of protein A (*Staphylococcus aureus*), an acidic model protein (IEP $\leq$ 5.1) on a sensor chip surface. A systematic evaluation of the correlation between DMEN derivatization and electrostatic preconcentration, protein immobilization, and nonspecific binding was conducted, and the performance of our approach was further validated using other acidic proteins, including pepsin.

We also found that the reversed-charge approach was useful for immobilizing nucleic acids. Concentration-dependent hybridization experiments of a ssDNA 16mer with its immobilized complementary strand were performed, and chip performance was compared with that of a biotinylated ssDNA sequence analog immobilized on a high-capacity streptavidin sensor chip. The significantly increased signal-to-noise ratios achieved with the reversed-charge modification further demonstrated the potential of this approach.

Materials and methods

Chemicals and consumables

PAA sensor chips (12 × 12 × 0.3 mm, 42-nm gold layer on glass coated with linear high-molecular-weight PAA) and streptavidin-coated sensor chips (SAD500M) were obtained from XanTec bioanalytics (Düsseldorf, Germany).

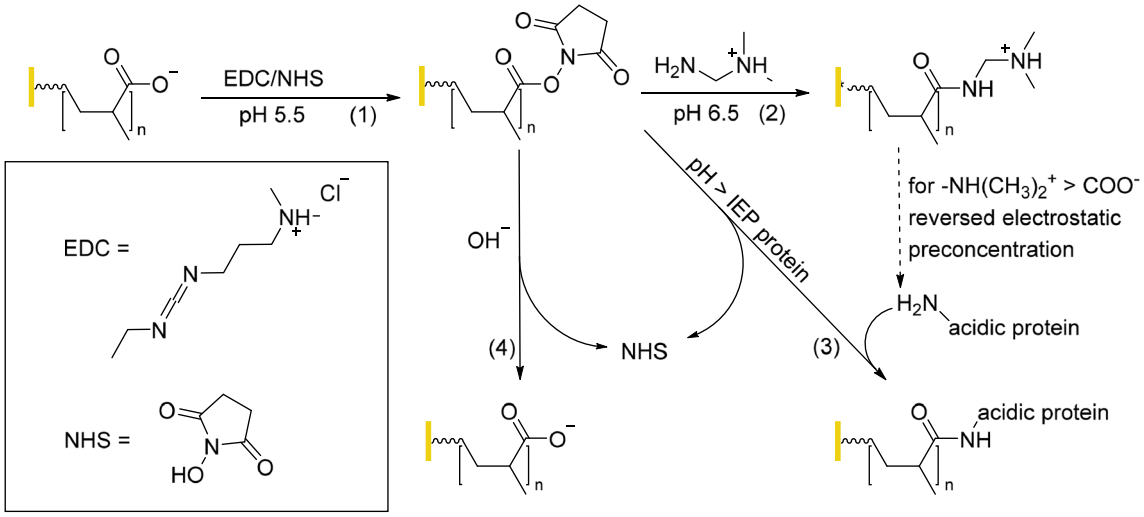

Scheme 1 Principle of the reversed-charge preconcentration approach on PAA-coated SPR chips. *(1)* Carboxylic groups activated by EDC/NHS chemistry. *(2)* NHS esters derivatized by reaction with DMEN, reverting the negative net charge of the sensor surface. *(3)* Acidic proteins preconcentrated at a pH above their IEP and covalently immobilized by remaining NHS esters. *(4)* Hydrolysis of unreacted NHS esters

Hydrochloric acid (HCl, 37%), sodium hydroxide (NaOH, 99%), sodium chloride (NaCl, 99%), and glycine (>99%) were purchased from Carl Roth (Karlsruhe, Germany). Formic acid (98%) was purchased from Fluka (Buchs, Switzerland). *N*,*N*-dimethylethylenediamine (DMEN, 99%), toluidine blue O (TBO, >95%), and orange II (>95%) were purchased from Acros (Geel, Belgium). Boric acid (99%), *N*-ethyl-*N*-(3-dimethylaminopropyl)carbodiimide hydrochloride (EDC, >99%), *N*-hydroxysuccinimide (NHS, 98%), 4-(2-hydroxyethyl)-1-piperazineethanesulfonic acid (HEPES, ≥99.5%), 2-(4-morpholino)ethanesulfonic acid (MES, ≥99%), bovine serum albumin fraction V (BSA, 99%), and lysozyme (>90%) were obtained from Sigma (St. Louis, MO, USA). Protein A (*Staphylococcus aureus*) (97% activity, IEP 4.85–5.10) was obtained from Prozyme (Hayward, CA, USA). Rabbit IgG (protein A purified) was obtained from ImmunoGlobe (Himmelstadt, Germany). DNA sequences for hybridization experiments were obtained from Integrated DNA Technologies (Coralville, IA, USA) and purified by HPLC (Table 1). All solutions and buffers were sterile filtered before use (0.22-μm filter).

Table 1 List of DNA sequences

Description	Sequence
Amino-ssDNA	NH_2-(C6)-GGCCGAAATTTGCCGG
Biot-ssDNA	Biot-(C6)- GGCCGAAATTTGCCGG
Anti-ssDNA	CCGGCAAATTTCGGCC

DMEN derivatization of PAA sensor chips

The sensor chips were incubated in alkaline elution buffer (2 M NaCl, pH 12) for 30 min and allowed to equilibrate for another 30 min in water. Derivatization with DMEN was performed as follows. A 1.5-mL solution containing 1 M DMEN, 100 mM MES, 100 mM NaCl, and 250 mM NHS at pH 6.5 was mixed with different concentrations of EDC (0–500 mM). The solution was applied to the sensor chips for 12 h. The chips were then consecutively immersed in 0.5 M NaOH, HBS (pH 7.4), and water for 30 min each. The sensor surfaces were dried under a stream of dry air and stored under an argon atmosphere at −25 °C until used.

In a second approach, activation and derivatization of the sensor surfaces were realized in two separate processing steps. First, the PAA SPR sensor chips were activated by a solution consisting of 100 mM MES (pH 5.5 or 6.5) or 100 mM MOPS (pH 7.5), 100 mM NaCl, 250 mM NHS, and 500 mM EDC for 10 min. Derivatization was then performed with a solution comprising 100 mM MES (pH 5.5 and 6.5) or 100 mM MOPS (pH 7.5), 100 mM NaCl, and 1 M DMEN for 2 h. Subsequent processing was identical to that described above for one-step derivatization.

Colorimetric quantification of carboxyl and tertiary amino group density

Carboxyl groups were quantified by the adsorption of cationic TBO dye using a procedure described in detail elsewhere [17,

18]. Briefly, the sensor chip was immersed in a solution of 0.5 mM TBO at pH 10 for 5 h, followed by the removal of unbound dye using a solution of 0.1 mM NaOH. Bound TBO was desorbed by applying 50% (v/v) acetic acid for 5 min. The absorbance of TBO in acetic acid solution was measured at 633 nm using a UV/vis spectrophotometer (Ultrospec 4000, Pharmacia (Pfizer), New York, NY, USA). The carboxyl group density was derived from a calibration curve obtained using defined quantities of TBO in 50% (v/v) acetic acid.

The $N(CH_3)_2$ groups were quantified by the adsorption of anionic Orange II dye [17, 19, 20]. The sensor chips were incubated for 5 h in a pH 3 solution of 0.5 mM Orange II. Uncomplexed dye was removed by washing with 1 mM HCl, while bound dye was extracted with 1 mM NaOH. Colorimetric evaluation was performed at 485 nm. A calibration plot of defined Orange II quantities in 1 mM NaOH was used to calculate the surface density; see Figs. S1 and S2 in the "Electronic supplementary material" (ESM) for the respective calibration plots.

ATR-FTIR measurements

Sensor chips were mounted in a Nicolet 6700 FTIR spectrometer (Thermo Fisher Scientific, Waltham, MA, USA) equipped with an attenuated total reflectance module (silicon prism). All sensor chips were fixed using the same pressure, with the coated surface oriented towards the silicon prism. Spectra were recorded with a resolution of 4 cm^{-1} using a photodiode detector. Air-referenced scans (72 in total) were performed for each of the surfaces. For each DMEN modification, three independent samples were analyzed. Data acquisition was realized using OMNIC software v.8.3.103 (Thermo Fisher Scientific).

SPR experiments

Preconcentration scouting

Preconcentration experiments were performed using an SR7500DC surface plasmon resonance dual channel spectrometer (Reichert, Buffalo, NY, USA). The instrument was equipped with a syringe pump (SR8500, Reichert), autosampler (SR7100, Reichert), diverter valve (SR8600 Reichert), and online degasser (DEG 100, XanTec). Data acquisition was performed using Integrated SPRAutolink software (Reichert), and data processing was performed using Tracedrawer software (Ridgeview Instruments, Vänge, Sweden). Adsorption experiments were realized under a continuous flow of 10 mM HEPES (pH 7) at 25 °C. Surfaces were primed for 10 min with an injection of 2 M NaCl at pH 12 (PAA sensor chips) or an additional consecutive 10-min injection of 2 M NaCl at pH 2 (DMEN-modified sensor chips). After equilibration for 20 min with running buffer, protein A solutions at various pH values (100 μg/mL protein A: 10 mM formic acid, pH 3.0–4.0; 10 mM acetic acid, pH 4.5–5.0; 10 mM MES, pH 5.5–6.5; 10 mM HEPES, pH 7.0; 10 mM boric acid, pH 8.0–10) were injected for 20 min. The sensor surface was regenerated by repeating the initial priming process. Protein A solutions were injected in random order. Two repetitions were performed for each surface type ($n = 3$).

In-situ reversed-charge preconcentration (ISRP) and immobilization

ISRP experiments were performed using a 4SPR surface plasmon resonance spectrometer with four channels (Reichert). A syringe pump, degasser unit, and diverter valve were already integrated, and the device was combined with an autosampler (SR7100, Reichert). Data acquisition and processing were performed using Integrated SPRAutolink 4 Channel software (Reichert) and Tracedrawer (Ridgeview Instruments), respectively. Protein A immobilization experiments on mounted PAA SPR sensor chips were carried out under a continuous flow of 10 mM MES (pH 6.5) at 25 °C. Initially, the sensor surface was primed with a 10-min injection of 2 M NaCl (pH 12) at 25 μL/min. The surface was allowed to equilibrate for 20 min with running buffer before activation was performed with a solution of 100 mM MES, 100 mM NaCl, 250 mM NHS, and 500 mM EDC at pH 5.5 (channels 1 and 2). EDC was added to the solution directly to minimize degradation, followed by sterile filtration (0.22-μm filter) before injection. Surface activation was allowed to proceed for 10 min at a flow rate of 25 μL/min. After a quick rinse with running buffer, DMEN solution (100 mM MES, 100 mM NaCl, 1000 mM DMEN, pH 6.5) was injected for various time periods (0–30 min) at a flow rate of 10 μL/min (channel 1 and 2). Subsequently, a solution of protein A (100 μg/mL in 10 mM MES, pH 6.5) was injected for 30 min at a flow rate of 10 μL/min (channel 1). Unbound protein A was removed and unreacted NHS esters were quenched by injecting 2 M NaCl (pH 12), 1 M ethanolamine (pH 8.5), and 2 M NaCl (pH 12) for 15 min each at a flow rate of 25 μL/min (all channels).

Nonspecific and specific protein binding of the previously modified sensor surfaces were analyzed using HBS (10 mM HEPES, 150 mM NaCl, pH 7.4) as running buffer. Again, the sensor surfaces were initially primed with an injection of 2 M NaCl (pH 12) for 10 min, followed by a 10-min injection of 2 M NaCl (pH 2) at 25 μL/min. After equilibration for 20 min with running buffer, a BSA solution (1 mg/mL in HBS) was injected for 15 min followed by another 15-min rinse with running buffer. Nonspecifically bound BSA was removed by repeating the priming procedure. Nonspecific lysozyme binding was assessed in the same way as nonspecific BSA binding. The amount of nonspecifically bound protein was calculated from the baseline shift from 10 s before injection to 15 min after injection. Specific binding was analyzed using a 40-min injection of a protein A purified IgG solution (100 μg/mL in HBS) at a flow rate of

10 μL/min. The amount of bound IgG was calculated from the baseline shift from 10 s before injection to the end of injection, and was referenced against channel 2. Regeneration was achieved with a 5-min injection of 50 mM glycine (pH 2). Two repetitions of DMEN incubation (20 min each) were used to estimate the reproducibility of the ISRP process.

DNA immobilization and hybridization Amino-ssDNA (10 μg/mL) was immobilized according to the ISRP and immobilization procedures described above (DMEN incubation time, 5 min), but with an additional 2-h buffer rinse (1 μL/min) after the preconcentration process. As soon as the immobilization sequence was completed, the running buffer was changed to phosphate-buffered saline (PBS; 10 mM phosphate, 150 mM NaCl, pH 7.4) and the surface was allowed to equilibrate. Afterwards, anti-ssDNA (1 μM) was pumped over the sensor surface for 10 min at 20 μL/min and 25 °C. The signal difference between channels 1 and 2 recorded 595 s after injection was started was taken as the report point, which was used to determine the maximum hybridization capacity.

The sensitivity of the ssDNA sensor surface was determined using a concentration-dependent hybridization experiment. Firstly, the sensor surface was primed with three injections of 10 mM NaOH for 5 min at 45 °C, followed by running buffer at 25 °C until a stable baseline was established. Next, five blank injections for 4 min at 25 μL/min, separated by 10 min of running buffer, were run as a second preliminary step. Subsequently, anti-ssDNA was injected for 4 min with the concentration increasing from 0 to 100 nM at 25 μL/min. Injections were separated by a 5-min rinse with running buffer. Regeneration was performed after injection of the highest DNA concentration (100 nM) using two 2-min injections of 10 mM NaOH for 10 min at 45 °C. Anti-ssDNA injection and subsequent regeneration was repeated twice to demonstrate assay reproducibility and surface stability. The double-referenced signals found 250 s after the start of injection were plotted against the sample concentration and linearly fitted to determine the sensitivity of the sensor surface. The limits of detection (LOD) and quantitation (LOQ) were defined as the concentrations that generated signals three and nine times the standard deviation (σ) of blank injections, respectively.

To compare the performance of the ISRP-derived DNA sensor, a commercially available high-capacity streptavidin-coated sensor chip based on a CMD matrix (SAD500M, XanTec) was employed. Firstly, the sensor chip was preconditioned with an injection of guanidine (6 M, pH 1.5) for 10 min at 25 μL/min and 25 °C to increase the baseline stability. PBS was used as the running buffer and immobilization was realized by injecting biot-ssDNA (10 μg/mL in PBS), followed by three 5-min injections of 5 mM HCl. Afterwards, the sensor matrix was allowed to stabilize overnight. Hybridization experiments were performed according to the procedure used for the ISRP approach, but with regeneration conducted using two 10-min injections of 5 mM HCl at 25 °C and no priming with 10 mM NaOH at 45 °C.

Results and discussion

The first part of this work aimed to identify the appropriate experimental conditions for EDC/NHS chemistry that would allow the derivatization of commercially available PAA-coated SPR sensor chips with DMEN. To change the net charge of the sensor matrix, a coupling yield of >50% was assumed to be essential. To achieve this goal, PAA sensor chips were derivatized as a function of EDC concentration making use of the one-step derivatization approach, and were analyzed accordingly using the methods described above.

Surface characterization by colorimetry

The DMEN-modified sensor chips were analyzed using two complementary colorimetric assays. The quantity of COOH groups was determined from TBO absorption, while the density of positive $N(CH_3)_2$ groups was derived from Orange II absorption, with the results shown in Fig. 1a. With increasing EDC concentration, the density of COOH groups continuously declined. In contrast, the density of $N(CH_3)_2$ groups constantly increased with increasing EDC concentration, reaching a maximum at 500 mM EDC. For EDC concentrations ≥250 mM, the $N(CH_3)_2$ density exceeded the COOH density. Moreover, the sum of functional group densities was not constant; it presented a minimum between 200 and 250 mM EDC. Accordingly, the density of functional groups was considered as apparent. This result was due to inner salt formation between COOH and $N(CH_3)_2$ groups, which competed with the adsorption of dye molecules, and was presumably most dominant at a 1:1 ratio of COOH and $N(CH_3)_2$. Furthermore, assuming that both functional groups competed with the adsorption of the respective dye to comparable extents, the coupling yield η (%) can be calculated as follows:

$$\Delta c_x = c_{x\ \mathrm{TBO}} - c_{x\ \mathrm{Orange}\ II} \tag{1}$$

$$\Delta c_{x'} = \Delta c_x + \Delta c_0 \tag{2}$$

$$\eta(\%) = \left(1 - \frac{\Delta c_{x'}}{\Delta c_{0'}}\right) \cdot 100, \tag{3}$$

where $c_{x\ \mathrm{TBO}}$ and $c_{x\ \mathrm{Orange\ II}}$ are the amounts of each dye bound (in nmol/cm^2) as a function of EDC concentration. As shown in Fig. 1b, the results indicate that for EDC concentrations ≥250 mM, a conversion rate of >50% was realized, leading to maximum coupling yield of 71 ± 3.3% at 500 mM EDC. These results are in good agreement with previous

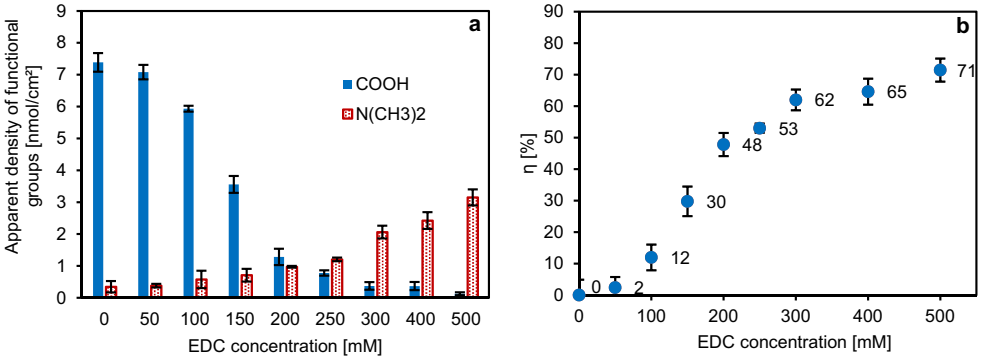

Fig. 1 **a** Apparent densities of COOH and $N(CH_3)_2$ groups as functions of the applied EDC concentration (one-step DMEN derivatization). *Bars* represent the mean values of three independently modified sensor chips. *Error bars* represent σ ($n = 3$). **b** Derivatization yield as a function of EDC concentration. *Error bars* represent combined σ ($n = 6$)

findings for PAA coatings, although the EDC/NHS ratios and concentrations deployed were different [16].

ATR-FTIR analysis

The results described above were further supported by complementary ATR-FTIR measurements, as shown in Fig. 2. Unmodified PAA sensor chips showed a strong and broad absorption band at 1590 cm^{-1} that was assigned to the ν COO^- vibrational band. With increasing EDC concentration, the intensity of the ν COO^- absorption band declined, leading to a final intensity of 36.3%, while two increasingly pronounced adsorption bands appeared at 1660 cm^{-1} and 1560 cm^{-1}, which were assigned to the amide I and amide II bands, respectively. Although it is tempting to correlate the derivatization yield directly with the decrease in the ν COO^- absorption band, this correlation would be affected by the increase in the amide II band with EDC concentration [16]. Consequently, coupling yields estimated from the decline in the ν COO^- absorption band tended to suffer from greater underestimation with increasing EDC concentration. Nonetheless, the results clearly show that for EDC concentrations ≥300 mM, a coupling yield of >50% was established, as only 42.5% of the initial ν COO^- peak intensity was found at this EDC concentration. Alternatively, at least 57.5% of the COOH groups were successfully converted to amides. For 500 mM EDC, a coupling yield of more than 63.4% was estimated. The results from FTIR analysis were in line with previously reported colorimetric surface quantification experiments (Fig. 1) which deduced a maximum coupling yield of 71 ± 3.3%. Therefore, it is likely that DMEN derivatization at high EDC concentrations (300–500 mM) caused charge reversal on the PAA sensor surfaces. Further confirmation of charge reversal was provided by zeta potential measurements (Fig. S3 in the ESM) and dynamic water contact angle measurements (Fig. S4 in the ESM).

Separation of activation and derivatization (two-step DMEN derivatization)

For the experiments described above, activation and derivatization were realized using a one-step approach. For the in-situ

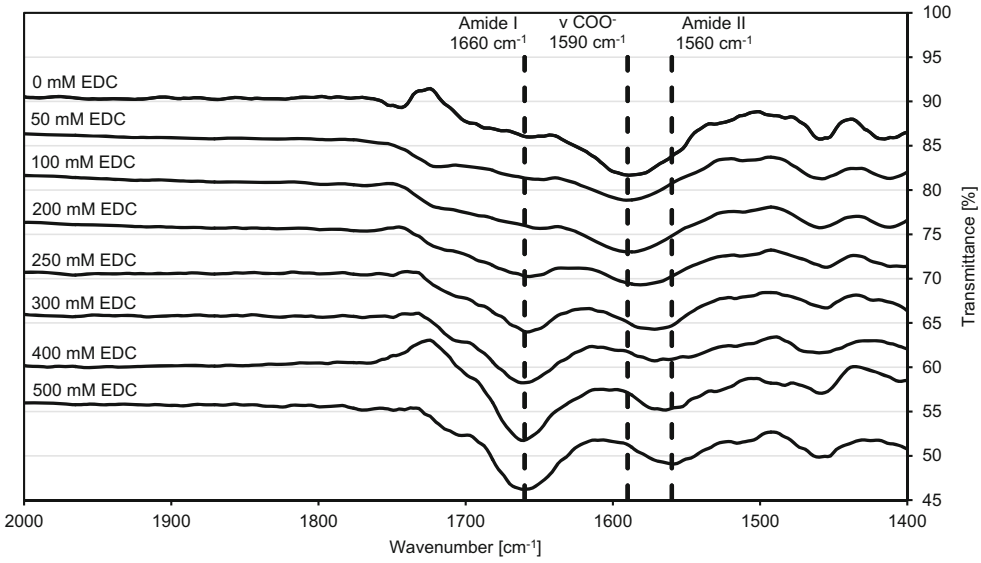

Fig. 2 Stacked ATR-FTIR spectra for DMEN-modified PAA sensor chips at different EDC concentrations (one-step DMEN derivatization). *Dashed lines* highlight relevant peaks

SPR derivatization of ligands, it may be preferable to separate activation and derivatization as it would improve process control. Furthermore, reaction times of 12 h are difficult to realize in commercially available SPR devices. Accordingly, a screening experiment was established in which EDC/NHS activation and derivatization with DMEN were separated while varying the respective pH values of the solutions. The results are shown in Fig. 3, which illustrates the apparent $N(CH_3)_2$ density.

For all conditions tested, Orange II absorption indicated a coupling yield of >50%. The highest immobilization yields were realized by combining activation at pH 5.5 with DMEN derivatization at pH 6.5. The activation pH had a greater effect than the derivatization pH on the derivatization yield, leading to a maximum conversion rate of 84.8% when using the one-batch approach with 500 mM EDC (Fig. 1). Furthermore, it was estimated that a high degree of COOH activation was established even after incubation for 10 min with EDC/NHS, while the DMEN incubation time was reduced to 120 min. The fast surface activation was in good agreement with previous reports [9, 21] and supported the concept of fully integrating a reversed-charge sensor matrix into an automated SPR immobilization routine.

SPR: electrostatic preconcentration on DMEN-modified sensor surfaces

The second part of this work explored whether the above derivatization procedure could be transferred to commercially available SPR devices for electrostatically preconcentrating acidic proteins in a negatively charged state and immobilizing them covalently on the sensor matrix. Accordingly, in-situ derivatization of PAA sensor chips with DMEN was performed and compared with the adsorption of protein A on unmodified PAA sensor chips at different pH values. The results of this procedure, known as preconcentration scouting, are shown in Fig. 4, with the quantity of immobilized protein A shown as a shift in refractive index (mRIU) as a function of pH. The blue values represent adsorbed quantities of protein A on bare PAA sensor chips, with the maximum adsorption of 17.6 ± 1.1 mRIU (1 μRIU = 10^{-3} mRIU = change in refractive index units of $10^{-6} \approx 1$ RU and 1 ng/mm^2 protein adsorption ≈ 1 mRIU) occurring at pH 5.0. Only relatively small adsorption densities were observed at pH values ≥6.0 (≤1.0 mRIU), while considerable adsorption was detected at pH 5.5 (12.1 mRIU). This result is remarkable because pH 5.5 is above the IEP of protein A (IEP 4.85–5.10), which should lead to repulsion, not electrostatic attraction, between negatively charged polyacrylate and protein A. Such adsorption on the wrong side of the protein's IEP can be explained by the charge anisotropy and charge regulation effects of the protein in the presence of surface-anchored polyelectrolytes with high electrostatic potentials, such as high molecular weight polyacrylic acid, and has been described in detail elsewhere [22–26]. In contrast to bare polyacrylic acid-coated sensor chips, DMEN-modified sensor chips showed their highest protein A adsorption at pH 6, resulting in a maximum adsorption of 26.2 ± 2.7 mRIU. This corresponded to a total increase in maximum electrostatic adsorption of 48.6% compared with bare PAA sensor chips, and demonstrated a dramatic 25-fold increase in electrostatically adsorbed protein A for $pH = IEP_{protein\ A} + 1$. Even at pH 8, as much as 5.3 ± 1.0 mRIU was adsorbed on the DMEN-modified sensor surface. This pH-dependent adsorption characteristic was likely due to charge reversal of

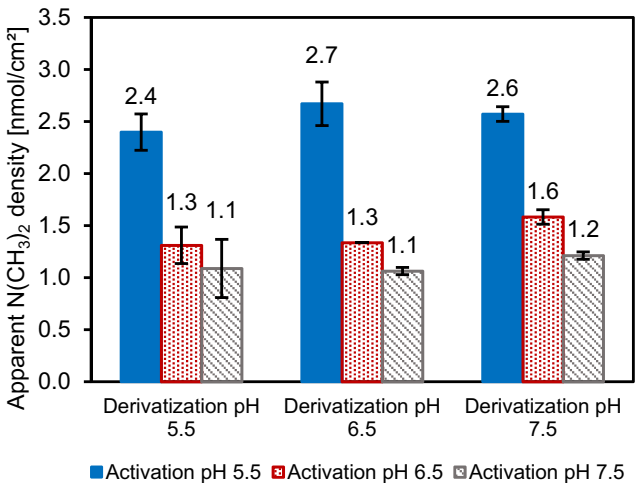

Fig. 3 Quantification of the apparent $N(CH_3)_2$ density as a function of pH in the activation and derivatization solutions. Activation was performed with 500 mM EDC. *Colored bars* represent the mean values of three samples. *Error bars* represent σ ($n = 3$)

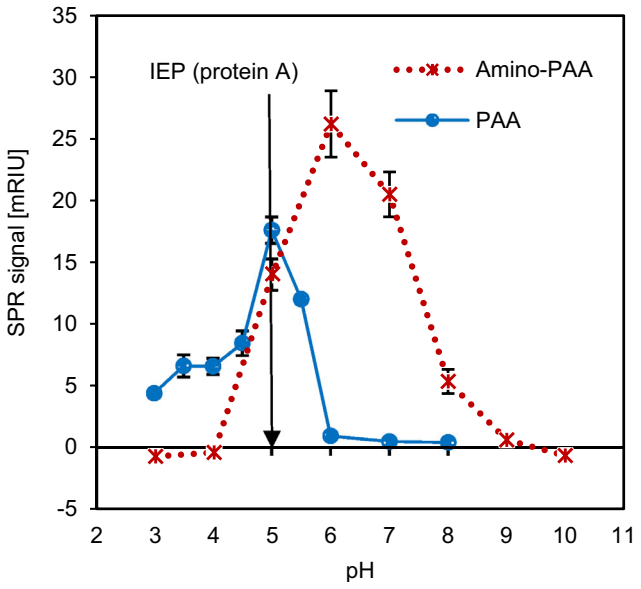

Fig. 4 Preconcentration scouting of protein A on PAA sensor chips (*blue dots*) and DMEN-modified PAA sensor chips (*red cross*) versus pH. Ionic strength was 10 mM at all pH values. Experiments were performed with three independent samples. *Error bars* represent σ ($n = 3$)

the PAA sensor chip for pH values <9, allowing effective protein adsorption in the pH range $IEP_{protein\ A} \leq pH \leq 8$. For pH values ≤ 4 and ≥ 9, electrostatic repulsion dominated the interaction between the sensor surface and protein A, for pH < $IEP_{protein\ A}$, both interactants had a positive net charge, and for pH ≥9 the sensor matrix probably lost this feature. Notably, at pH 3, 4, and 10, the SPR response was negative. A possible explanation for the observed negative SPR shifts could be the appearance of matrix effects. Specifically, electrostatic repulsion at these pH values may cause the polymer chains to stretch because most COOH groups are uncharged in acidic conditions (pH ≤4) and the positive $NH(CH_3)_2^+$ groups repel each other. Under alkaline conditions (pH ≥10), this effect is reversed, because uncharged $N(CH_3)_2$ groups cannot form salt bridges with COO^- groups, resulting in electrostatic repulsion between the charged carboxyl groups, which is associated with polymer chain stretching. At pH 4–9, salt bridges between COO^- and $NH(CH_3)_2^+$ groups lead to attraction between the surface-bound polymer chains [27].

The electrostatic adsorption experiments illustrated in Fig. 4 clearly showed that the DMEN-modified PAA sensor chips caused a remarkable increase in protein A preconcentration at pH 1–2 above the IEP. Considering the preconcentration scouting of the bare PAA sensor chips, this pH shift in maximum protein A adsorption was most likely due to charge reversal of the sensor surface. However, as this binding is only electrostatic, a high ionic strength or extreme pH conditions can easily lead to quantitative removal of the bound protein. To achieve stable covalent immobilization of electrostatically preconcentrated ligands, amine coupling with the ligand was integrated into our approach.

SPR: in-situ immobilization by reversed-charge preconcentration

A possible method for combining preconcentration reversal and covalent immobilization is shown in Fig. 5. First, the PAA sensor chip was activated with EDC/NHS for 10 min, which had already been found to be sufficient time (Fig. 3). Subsequently, the surface was modified with DMEN for another 10 min, followed by an injection of protein A. As shown in Fig. 5, the DMEN derivatization efficiency was adequate to reverse the charge of the sensor matrix, as demonstrated by the electrostatic adsorption of protein A at pH 6.5. After the deactivation and desorption of protein A with a solution of 2 M NaCl (pH 12), the amount of covalently immobilized ligand was verified. In the example shown in Fig. 5, 22.9 mRIU of protein A was electrostatically adsorbed, while as much as 15.6 mRIU (68%) was successfully immobilized covalently. The covalent immobilization of protein A can be explained by the incomplete conversion of activated COOH groups. Although the derivatization efficiency with DMEN was sufficiently high to reverse the net charge of the sensor surface, the density of unreacted NHS esters was adequate for protein A coupling.

Having demonstrated the feasibility of combining the reversed-charge preconcentration with EDC/NHS coupling, further experiments were performed to investigate the impact of DMEN incubation time on protein A immobilization. The results are shown in Table 2 and Fig. 6. Increasing DMEN incubation time was estimated to correlate with the positive charge density of the sensor matrix within a certain timeframe, resulting in an increase in the preconcentration level of protein

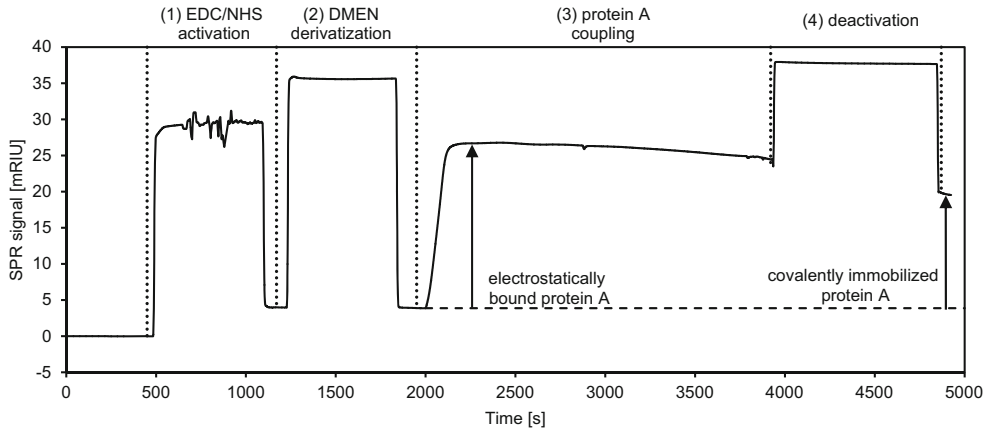

Fig. 5 SPR sensorgram showing the complete in-situ reversed-charge preconcentration (ISRP) and immobilization of protein A on a PAA SPR sensor chip. *(1)* Sensor chip surface was activated with a solution of 500 mM EDC and 250 mM NHS (pH 5.5). *(2)* Activated COOH groups reacted incompletely with DMEN (1 M, pH 6.5), reversing the surface charge. *(3)* Electrostatically bound protein A was reacted for 30 min with the remaining activated COOH groups at pH 6.5. *(4)* Alkaline hydrolysis of activated COOH groups (2 M NaCl, pH 12) and the removal of noncovalently bound protein A. Artifacts that occurred shortly after the injection of the EDC/NHS solution can be attributed to emerging gas bubbles that were observed in the transparent tubing system of the SPR device. As EDC/NHS chemistry generally does not produce any gaseous byproducts, it is likely that trace amounts of ethyl isocyanate (one of the educts of EDC synthesis) reacts in a way that leads to gas bubbles at high EDC concentrations [28]. These gas bubbles were conveniently removed using a short pulse of running buffer (200 μL/min) following activation

Table 2 Immobilization characteristics of protein A on PAA sensor chips versus DMEN incubation time

DMEN incubation (min)	Protein A, electrostatic (mRIU)	Protein A, covalent (mRIU)	Nonspecific binding of lysozyme (μRIU)	Nonspecific binding of BSA (μRIU)	Specific binding of IgG (mRIU)	Yield [b]
0	0.251	0.246	26,117	−6	0.02	0.98
1	14.47	14.01	62	5	9.95	0.97
5	19.25	18.46	0	49	16.42	0.96
10	22.89	15.58	0	98	20.14	0.68
15	25.13	10.99	19	452	23.36	0.44
20	25.79 ± 0.28	7.94 ± 0.51	13 ± 11	827 ± 24	24.16 ± 0.31	0.31 ± 0.02
25	26.52	5.69	59	1603	21.75	0.21
30	26.09	4.37	49	2178	20.32	0.17
Error (%) [a]	1.10	6.36	86.69	2.90	1.26	5.54

Activation, DMEN derivatization, and protein A coupling were conducted at pH 5.5, 6.5, and 6.5, respectively

[a] Errors represent coefficients of variation of three independent repetitions at a DMEN incubation time of 20 min

[b] Yield is defined as the amount of covalently bound protein A divided by the amount of electrostatically bound protein A

A. A plateau was reached after approximately 20 min of incubation regarding the amount of preconcentrated protein, while the actual covalent coupling yields of protein A declined for DMEN incubation times of >20 min. Moreover, the amount of electrostatically bound protein A at a DMEN incubation time of 20 min (25.8 mRIU) nearly equaled that of the preconcentration scouting experiment with DMEN shown in Fig. 4 (incubation time, 2 h; pH 6; 26.2 mRIU). This led to the conclusion that the positive charge density of the sensor surface did not contribute to protein A adsorption beyond a certain level, and that the adsorption density was limited due to steric effects. In contrast to electrostatic adsorption, the coupling yield (the amount of covalently bound protein divided by the amount of electrostatically bound protein) tended to decrease continuously, probably because increasing the DMEN incubation time led to continuous depletion of reactive esters, preventing their subsequent reaction with protein A.

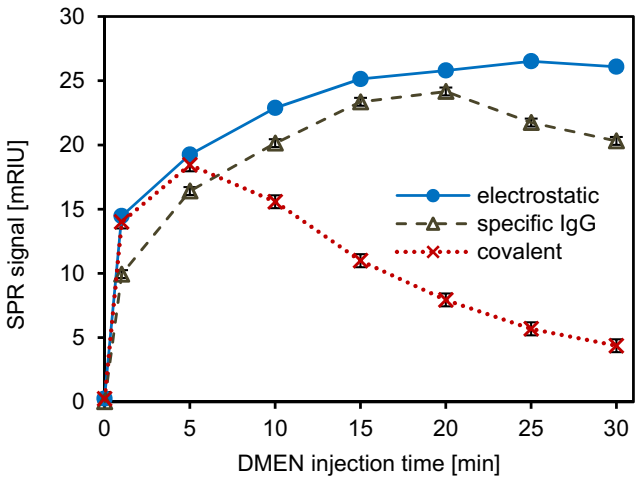

Fig. 6 Amounts of electrostatically adsorbed (pH 6.5, *blue dots*) and covalently bound (*red crosses*) protein A and specifically bound rabbit IgG (pH 7.4, *gray triangles*) as functions of DMEN incubation time. *Error bars* represent σ at a DMEN incubation time of 20 min ($n = 3$)

Notably, for short derivatization times (1 and 5 min), electrostatically bound protein A was near-quantitatively coupled with the sensor matrix (yields of 97% and 96%, respectively), assuming that a high density of activated carboxyl groups was present. These yields were higher than those observed on CMD surfaces, even under optimized conditions [9]. Moreover, charge reversal was found to be a fast process; even after 1 min, as much as 14.0 mRIU of protein A were electrostatically bound to the reversed-charge sensor surface. Activation was thought to have already caused a pronounced reduction in initial charge density, as neither NHS esters nor anhydride side products are ionic. Therefore, minor DMEN derivatization yields of <50% may be sufficient for temporary charge reversal.

Consecutive IgG binding to protein-A-modified sensor surfaces was used to confirm their activity. An increase was observed before a maximum was reached at a DMEN incubation time of 20 min (see adsorption isotherms in Fig. S5 of the ESM). This is an interesting observation because the amount of covalently bound protein A constantly decreased when using DMEN incubation times of >5 min and, intuitively, one would also expect a decrease in IgG binding in this situation. This apparent contradiction can be explained by steric hindrance due to multiple binding of protein A molecules. Though the initial activation level was identical for all DMEN incubations, the density of reactive NHS esters directly before the start of protein A injection was closely related to DMEN incubation, because shorter incubation times resulted in the less consumption of the NHS esters. Accordingly, the risk of multisite binding was highest for low DMEN injection times.

As surface charge is also an important factor in nonspecific protein adsorption, and is consequently a critical influence on sensor surface performance, BSA and lysozyme adsorption

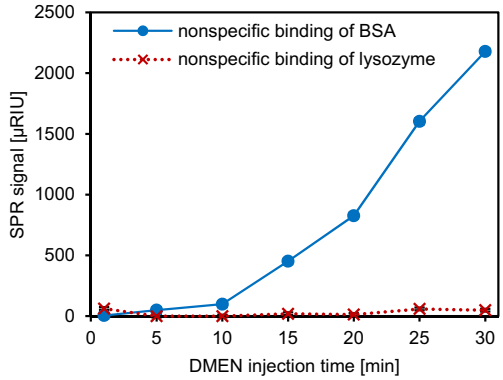

Fig. 7 Nonspecific adsorption of BSA (*blue circles*) and lysozyme (*red crosses*) on protein-A-modified PAA sensor chips as functions of DMEN incubation time. HBS was used as running buffer. *Error bars* represent σ at a DMEN incubation time of 20 min ($n = 3$)

were examined for all of the DMEN incubation times investigated. The results are shown in Table 2 and Fig. 7. Nonspecific lysozyme adsorption was low for all DMEN incubation times, showing a maximum response of 62 µRIU at 1 min, indicating that a neutral or positive net surface charge minimized electrostatic binding in HBS. As BSA is negatively charged at pH 7.4 (IEP 4.9), adsorption correlated with increasing derivatization time, resulting in a maximum of 2.2 mRIU at a DMEN incubation time of 30 min.

However, short derivatization times of 1 and 5 min showed low nonspecific adsorption, with total values of 67 and 49 µRIU for BSA and 60 and 0 µRIU for lysozyme, respectively. These remarkable results can be explained by the presence of a net surface charge of close to zero, as positively and negatively charged moieties are assumed to exist in an approximate 1:1 ratio on the surface (see Figs. S6 and S7 in the ESM for the nonspecific protein adsorption of the DMEN-only modified reference channel 2). These types of polyampholytic surface coatings, consisting of equal amounts of weakly acidic and basic functional groups, are known to exhibit excellent bioinertness at physiological pH values in the presence of a wide variety of proteins, which would explain our findings [29–31]. However, a charge-neutral polyampholyte only allows low-level electrostatic preconcentration of proteins [32]. Consequently, these surfaces generally do not allow high immobilization yields with EDC/NHS, if they are applicable at all.

Considering the results shown in Figs. 6 and 7, a DMEN incubation time of 5 min clearly yielded the best balance between coupling yield and nonspecific protein binding. The only negative aspect associated with this incubation time—reduced ligand activity due to assumed multisite binding—should be easy to control by reducing the ligand incubation time. In the ESM (Fig. S7 and Table S1), the results of additional test immobilizations performed with various acidic proteins (including the highly acidic pepsin, IEP 2.0–2.5) using the favored DMEN incubation time of 5 min are presented; those results demonstrate the general applicability of the reversed-charge approach. However, the types of sensor matrices that are compatible may be limited, as charge reversal on CMD sensor chips failed (see Fig. S9 in the ESM).

SPR: reversed-charge preconcentration and immobilization of ssDNA

The experiments with protein A demonstrated the feasibility of ISRP and amine coupling. Nevertheless, protein A has already been successfully immobilized on state-of-the-art CMD sensor chips using classic EDC/NHS chemistry without charge reversal [9, 33]. One class of biomolecules that are not accessible using preconcentration with subsequent EDC/NHS coupling are nucleic acids (including related aptamers), because the high negative charge density of the phosphate backbone does not allow electrostatic preconcentration on negatively charged substrates. Consequently, successful immobilization of nucleic acids would validate the performance of our newly developed concept. Figure 8 shows the immobilization of an amino-modified 16mer ssDNA oligo using the general procedure established for protein A. Indeed, the amino-ssDNA was successfully preconcentrated (6.28 mRIU) and immobilized (2.53 mRIU) using the reversed-charge approach, affording a

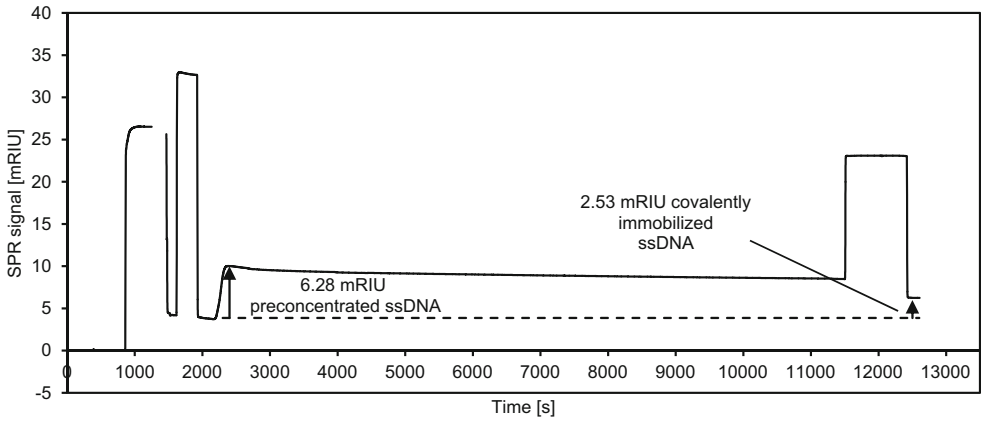

Fig. 8 SPR sensorgram showing in-situ reversed-charge preconcentration and immobilization of amino-modified 16mer ssDNA on a PAA sensor chip. In contrast to the standard immobilization protocol applied to protein A, the immobilization time was prolonged to 150 min

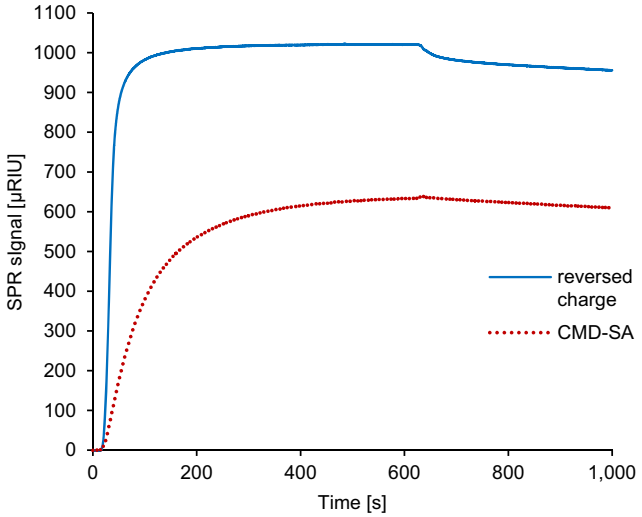

Fig. 9 SPR sensorgram showing the hybridization of anti-ssDNA (1 µM) with its complementary ssDNA, immobilized using the ISRP approach (*blue line*) or on a streptavidin-coated CMD chip (*red dotted line*)

coupling yield of 40.3%, which clearly demonstrates that our method can be applied to this important group of acidic ligands.

To further verify the success of reversed-charge immobilization, a hybridization experiment with the complementary DNA sequence (anti-ssDNA) was performed and compared to a biotinylated ssDNA analog coupled to a CMD sensor chip and preimmobilized with streptavidin. The resulting hybridization isotherms are shown in Fig. 9. The total amount of bound anti-ssDNA was 59% higher than that on the streptavidin chip. Considering 2.21 mRIU of immobilized biot-ssDNA (see Fig. S10 in the ESM), the activities of both approaches corresponded to 40.0% (reversed-charge) and 28.8% (streptavidin). Additionally, the shapes of the adsorption isotherms were markedly different from each other. The slope of the binding isotherm generated using the reversed-charge matrix was considerably steeper, which indicates a higher association rate. The different characteristics of the binding isotherms can be explained by the differing nanoarchitectures of the sensor matrices. EDC/NHS chemistry can generate multiple covalent bonds between reactive amine residues of proteins and the CMD sensor matrix, which may result in crosslinking, limiting diffusion through the sensor matrix [34, 35]. Indeed, Yang et al. have shown that the hybridization kinetics with biotinylated ssDNA immobilized on a CMD-based 3D streptavidin chip are strongly affected by the sensor matrix when compared

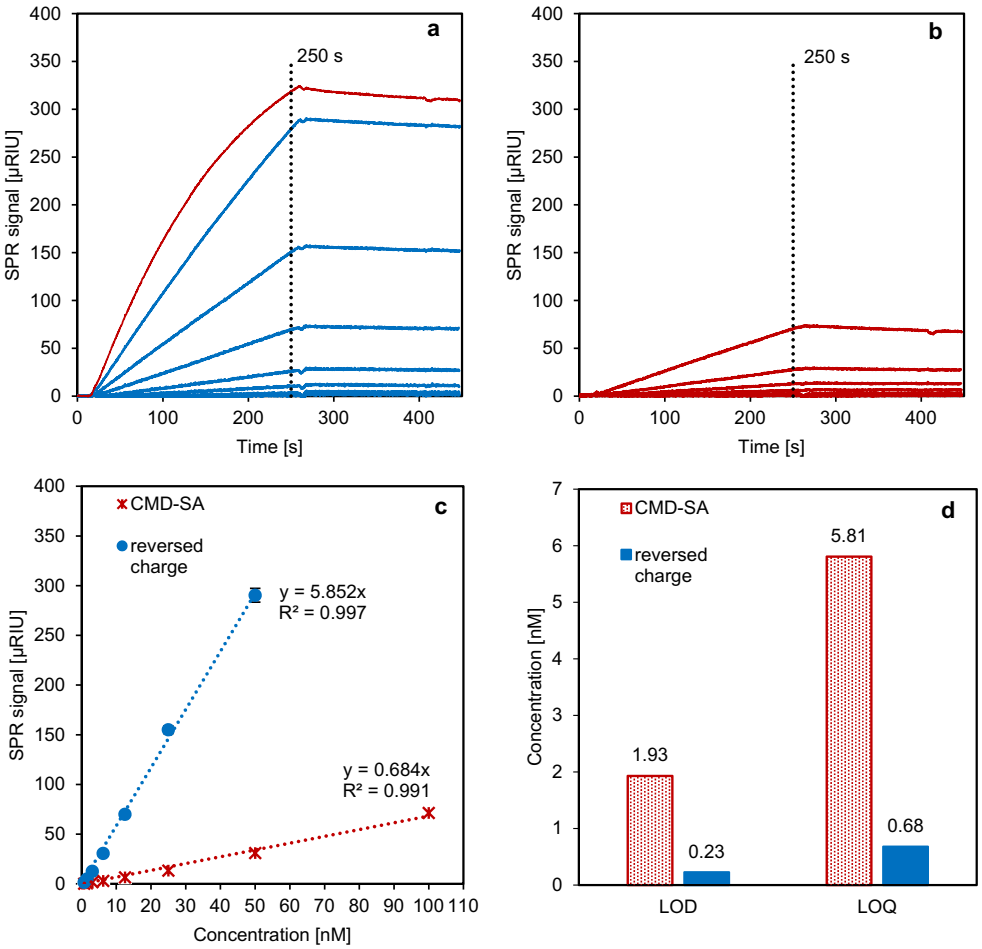

Fig. 10 **a**–**d** Sensorgrams of hybridization isotherms at anti-ssDNA concentrations of 0.78–100 nM performed for ssDNA sensor chips based on **a** ISRP immobilization and **b** streptavidin immobilization. **c** Concentration–response curve of the SPR signal at 250 s ($n = 3$) for each immobilization strategy (*blue dots* ISRP, *red crosses* streptavidin); sensitivity was derived from the slope of the linear fit and σ from six blank injections. **d** LOD and LOQ for each sensor chip

with a flat 2D coating [36]. In contrast, the PAA sensor chip provided a more open and flexible backbone with less steric hindrance, presumably resulting in easier diffusion and a higher apparent association rate.

Applications where higher apparent association rates may be a beneficial feature include those associated with analyte quantification. These binding assays rely on complex formation between the ligand and analyte, which is dominated by mass transport limitation (MTL). Under MTL, the increase in signal observed during analyte injection shows no curvature, and the slope of the SPR signal can be directly correlated with the analyte concentration [37]. Consequently, a higher apparent association rate should lead to increased sensitivity as long as diffusion limitation dominates the binding characteristics.

To gauge the performance improvement of SPR-related quantification experiments achieved when using DNA immobilization based on the reversed-charge approach, we conducted a series of hybridization experiments with analyte concentrations of 0.78–100 nM for comparison with the streptavidin-based DNA chip. The related sensorgrams are shown in Fig. 10a and b. Except for the binding isotherm of the ISRP ssDNA chip at an analyte concentration of 100 nM, all association curves showed a linear slope typical of MTL-controlled binding kinetics, which demonstrated that the binding isotherms of the reversed-charge chip had a significantly higher concentration-dependent signal increase. Plotting the signal after a certain interval (250 s) against the concentration and applying a linear fit is another method that can illustrate this difference (Fig. 10c). Remarkably, the fit attributed to the reversed-charge sensor chip had a slope that was 8.5 times steeper than that for the streptavidin sensor. Consequently, the ISRP chip also provided 8.5 times higher sensitivity, leading to a LOD of 0.23 nM and a LOQ of 0.68 nM (Fig. 10d). Compared to coating strategies that rely on planar 2D coatings, the reversed-charge DNA chip showed 44- to 630-fold higher sensitivity [38, 39]. In addition to this improved sensitivity, the results also supported our assumption that the diffusion limitation of the PAA sensor chip with the reversed-charge approach was less pronounced than that of the high-capacity streptavidin-coated CMD. This could be an important feature that requires further detailed investigation, because bulky CMD-based sensor coatings—especially those immobilized with streptavidin—have been shown to affect binding kinetics in many cases [34, 35, 37, 40, 41].

Conclusion

We have presented a convenient approach for overcoming the limitations of amine coupling in the immobilization of acidic proteins on polycarboxylate hydrogel sensor coatings. This approach employs an EDC/NHS-mediated charge reversal of PAA sensor chips, which allows electrostatic preconcentration of acidic proteins comprising a negative net charge. Protein A immobilization experiments demonstrated the feasibility of our reversed-charge approach, leading to excellent covalent immobilization yields. Furthermore, the successful amine coupling of various acidic proteins, including highly acidic pepsin, which was previously inaccessible using amine coupling on polycarboxylate hydrogels, demonstrated the potential of this concept.

In addition to excellent coupling efficiency, the process parameters of this method were easily adjusted by varying the DMEN incubation time, affording high immobilization yields along with low nonspecific binding characteristics. Remarkably, nonspecific binding was low in the presence of negative and positively charged proteins. In addition to its broad applicability with respect to protein coupling, this method was successfully transferred to the immobilization of amino-modified nucleic acids, an important class of anionic biomolecules that could not previously be preconcentrated on anionic substrates. Moreover, in an ssDNA quantification experiment, immobilization based on charge reversal showed superior performance to a state-of-the-art high-capacity streptavidin sensor chip. Further efforts are needed to verify the general applicability of this method to anionic carbohydrates and short oligopeptides. We are convinced that the relevance of our approach is not restricted to SPR sensor surfaces. The immobilization of high-density surface-bound negatively charged effector molecules and the pronounced bioinertness of the underlying support is an attractive combination that could prove beneficial in many other bioanalytical and biomedical applications.

Acknowledgements We would like to thank Dipl. Ing. Joachim Horst for his help with ATR-FTIR analysis.

Compliance with ethical standards

Conflict of interest Erk T. Gedig is MD of XanTec bioanalytics GmbH. Fabian Risse is financially supported by XanTec bioanalytics GmbH. Jochen S. Gutmann declares that he has no conflict of interest.

References

1. Bonnerjea J, Oh S, Hoare M, Dunnill P. Protein purification: the right step at the right time. Nat Biotech. 1986;4:954–8. https://doi.org/10.1038/nbt1186-954.
2. Peterson EA, Sober HA. Chromatography of proteins. I. Cellulose ion-exchange adsorbents. J Am Chem Soc. 1956;78:751–5. https://doi.org/10.1021/ja01585a016.

3. Fritz JS. Ion chromatography. Anal Chem. 1987;59:335A–44A. https://doi.org/10.1021/ac00131a002.
4. Liedberg B, Nylander C, Lundström I. Biosensing with surface plasmon resonance—how it all started. Biosens Bioelectron. 1995;10:i–ix. https://doi.org/10.1016/0956-5663(95)96965-2.
5. Nguyen HH, Park J, Kang S, Kim M. Surface plasmon resonance: a versatile technique for biosensor applications. Sensors. 2015;15:10481–510. https://doi.org/10.3390/s150510481.
6. Kretschmann E, Raether H. Notizen: radiative decay of non radiative surface plasmons excited by light. Z Naturforsch A. 2014;23:2135–6. https://doi.org/10.1515/zna-1968-1247.
7. Cooper MA. Optical biosensors in drug discovery. Nat Rev Drug Discov. 2002;1:515–28. https://doi.org/10.1038/nrd838.
8. Löfås S, Johnsson B. A novel hydrogel matrix on gold surfaces in surface plasmon resonance sensors for fast and efficient covalent immobilization of ligands. Chem Commun. 1990;1526–8. https://doi.org/10.1039/C39900001526.
9. Johnsson B, Löfås S, Lindquist G. Immobilization of proteins to a carboxymethyldextran-modified gold surface for biospecific interaction analysis in surface plasmon resonance sensors. Anal Biochem. 1991;198:268–77. https://doi.org/10.1016/0003-2697(91)90424-R.
10. Masson J-F, Battaglia TM, Davidson MJ, Kim Y-C, Prakash AMC, Beaudoin S, et al. Biocompatible polymers for antibody support on gold surfaces. Talanta. 2005;67:918–25. https://doi.org/10.1016/j.talanta.2005.04.023.
11. Rich RL, Myszka DG. Survey of the year 2003 commercial optical biosensor literature. J Mol Recognit. 2005;16:351–82. https://doi.org/10.1002/jmr.726.
12. Cuatrecasas P, Parikh I. Adsorbents for affinity chromatography. Use of *N*-hydroxysuccinimide esters of agarose. Biochemistry. 1972;11:2291–9. https://doi.org/10.1021/bi00762a013.
13. Balamurugan S, Obubuafo A, Soper SA, McCarley RL, Spivak DA. Designing highly specific biosensing surfaces using aptamer monolayers on gold. Langmuir. 2006;22:6446–53. https://doi.org/10.1021/la060222w.
14. Bang GS, Cho S, Kim B-G. A novel electrochemical detection method for aptamer biosensors. Biosens Bioelectron. 2005;21:863–70. https://doi.org/10.1016/j.bios.2005.02.002.
15. Freyer MW, Buscaglia R, Nguyen B, David Wilson W, Lewis EA. Binding of netropsin and 4,6-diamidino-2-phenylindole to an A2T2 DNA hairpin: a comparison of biophysical techniques. Anal Biochem. 2006;355:259–66. https://doi.org/10.1016/j.ab.2006.04.049.
16. Wang C, Yan Q, Liu H-B, Zhou X-H, Xiao S-J. Different EDC/NHS activation mechanisms between PAA and PMAA brushes and the following amidation reactions. Langmuir. 2011;27:12058–68. https://doi.org/10.1021/la202267p.
17. Sano S, Kato K, Ikada Y. Introduction of functional groups onto the surface of polyethylene for protein immobilization. Biomaterials. 1993;14:817–22. https://doi.org/10.1016/0142-9612(93)90003-K.
18. Tiraferri A, Elimelech M. Direct quantification of negatively charged functional groups on membrane surfaces. J Membr Sci. 2012;389:499–508. https://doi.org/10.1016/j.memsci.2011.11.018.
19. Uchida E, Uyama Y, Ikada Y. Sorption of low-molecular-weight anions into thin polycation layers grafted onto a film. Langmuir. 1993;9:1121–4. https://doi.org/10.1021/la00028a040.
20. Noel S, Liberelle B, Robitaille L, De Crescenzo G. Quantification of primary amine groups available for subsequent biofunctionalization of polymer surfaces. Bioconjugate Chem. 2011;22:1690–9. https://doi.org/10.1021/bc200259c.
21. Touahir L, Chazalviel J-N, Sam S, Moraillon A, Henry de Villeneuve C, Allongue P, et al. Kinetics of activation of carboxyls to succinimidyl ester groups in monolayers grafted on silicon: an in situ real-time infrared spectroscopy study. J Phys Chem C. 2011;115:6782−7. https://doi.org/10.1021/jp200150m.
22. Hu Y, Cao D. Adsorption of nonuniformly charged fullerene-like nanoparticles on planar polyelectrolyte brushes in aqueous solutions. Langmuir. 2009;25:4965–72. https://doi.org/10.1021/la804302q.
23. De Vos WM, Biesheuvel PM, de Keizer A, Kleijn JM, Cohen Stuart MA. Adsorption of the protein bovine serum albumin in a planar poly(acrylic acid) brush layer as measured by optical reflectometry. Langmuir. 2008;24:6575–84. https://doi.org/10.1021/la8006469.
24. Biesheuvel PM, Wittemann A. A modified box model including charge regulation for protein adsorption in a spherical polyelectrolyte brush. J Phys Chem B. 2005;109:4209–14. https://doi.org/10.1021/jp0452812.
25. De Vos WM, Leermakers FAM, de Keizer A, Cohen Stuart MA, Kleijn JM. Field theoretical analysis of driving forces for the uptake of proteins by like-charged polyelectrolyte brushes: effects of charge regulation and patchiness. Langmuir. 2010;26:249–59. https://doi.org/10.1021/la902079u.
26. Wittemann A, Ballauff M. Interaction of proteins with linear polyelectrolytes and spherical polyelectrolyte brushes in aqueous solution. Phys Chem Chem Phys. 2006;8:5269–75. https://doi.org/10.1039/B609879G.
27. Paynter S, Russell DA. Surface plasmon resonance measurement of pH-induced responses of immobilized biomolecules: conformational change or electrostatic interaction effects? Anal Biochem. 2002;309:85–95. https://doi.org/10.1016/S0003-2697(02)00255-5.
28. Sheehan J, Cruickshank P, Boshart G. Notes—a convenient synthesis of water-soluble carbodiimides. J Org Chem. 1961;26:2525–8. https://doi.org/10.1021/jo01351a600.
29. Bernards MT, Cheng G, Zhang Z, Chen S, Jiang S. Nonfouling polymer brushes via surface-initiated two-component atom transfer radical polymerization. Macromolecules. 2008;41:4216–9. https://doi.org/10.1021/ma800185y.
30. Li G, Xue H, Gao C, Zhang F, Jiang S. Nonfouling polyampholytes from an ion-pair comonomer with biomimetic adhesive groups. Macromolecules. 2010;43:14–6. https://doi.org/10.1021/ma902029s.
31. Chen S, Zheng J, Li L, Jiang S. Strong resistance of phosphorylcholine self-assembled monolayers to protein adsorption: insights into nonfouling properties of zwitterionic materials. J Am Chem Soc. 2005;127:14473–8. https://doi.org/10.1021/ja054169u.
32. Tah T, Bernards MT. Nonfouling polyampholyte polymer brushes with protein conjugation capacity. Colloids Surf B. 2012;93:195–201. https://doi.org/10.1016/j.colsurfb.2012.01.004.
33. Bennett D, Morton T, Breen A, Hertzberg R, Cusimano D, Appelbaum E, et al. Kinetic characterization of the interaction of biotinylated human interleukin 5 with an Fc chimera of its receptor α subunit and development of an ELISA screening assay using real-time interaction biosensor analysis. J Mol Recognit. 1995;8:52–8. https://doi.org/10.1002/jmr.300080109.
34. Karlsson R, Roos H, Fägerstam L, Persson B. Kinetic and concentration analysis using BIA technology. Methods. 1994;6:99–110. https://doi.org/10.1006/meth.1994.1013.
35. Edwards PR, Gill A, Pollardknight DV, Hoare M, Buckle PE, Lowe PA, et al. Kinetics of protein-protein interactions at the surface of an optical biosensor. Anal Biochem. 1995;231:210–7. https://doi.org/10.1006/abio.1995.1522.
36. Yang N, Su X, Tjong V, Knoll W. Evaluation of two- and three-dimensional streptavidin binding platforms for surface plasmon resonance spectroscopy studies of DNA hybridization and protein–DNA binding. Biosens Bioelectron. 2007;22:2700–6. https://doi.org/10.1016/j.bios.2006.11.012.
37. Karlsson R, Fält A. Experimental design for kinetic analysis of protein-protein interactions with surface plasmon resonance

biosensors. J Immunol Methods. 1997;200:121–33. https://doi.org/10.1016/S0022-1759(96)00195-0.
38. Su X, Wu Y-J, Knoll W. Comparison of surface plasmon resonance spectroscopy and quartz crystal microbalance techniques for studying DNA assembly and hybridization. Biosens Bioelectron. 2005;21:719–26. https://doi.org/10.1016/j.bios.2005.01.006.
39. Kai E, Sawata S, Ikebukuro K, Iida T, Honda T, Karube I. Detection of PCR products in solution using surface plasmon resonance. Anal Chem. 1999;71:796–800. https://doi.org/10.1021/ac9807161.
40. Drake AW, Tang ML, Papalia GA, Landes G, Haak-Frendscho M, Klakamp SL. Biacore surface matrix effects on the binding kinetics and affinity of an antigen/antibody complex. Anal Biochem. 2012;429:58–69. https://doi.org/10.1016/j.ab.2012.06.024.
41. Nguyen B, Tanious FA, Wilson WD. Biosensor-surface plasmon resonance: quantitative analysis of small molecule–nucleic acid interactions. Methods. 2007;42:150–61. https://doi.org/10.1016/j.ymeth.2006.09.009.

Fabian Risse is a research scientist at the R&D Department of XanTec bioanalytics GmbH, Germany, and a Ph.D. student at the Department of Chemistry of the University of Duisburg-Essen, Germany. He is working on the development and functionalization of polymer-based biosensor coatings and novel biocompatible coatings for biomedical applications.

Erk Gedig is CEO and cofounder of XanTec bioanalytics GmbH, a company that develops and manufactures biochips for the label-free analysis of biomolecular interactions. Before he joined XanTec, he received his M.Sc. from the University of Muenster, Germany, and served as research associate with the Institute of Chemical and Biochemical Sensor Research (ICB), where he developed biosensors and biocompatible coatings. He is author of several publications, book contributions, and patents in the field of optical and electrochemical biosensors, microfluidics, fluorophore technology, and surface science.

Jochen S. Gutmann is a professor at the Department of Chemistry of the University of Duisburg-Essen, Germany, and the CEO of the Textile Research Institute (DTNW) in Krefeld, Germany. He is working on the functionalization and characterization of polymer surfaces with polymer brushes, hydrogels, block copolymers, and polyelectrolytes in order to achieve novel functional materials via tailored surface modification.